Monthly Notices of the ROYAL ASTRONOMICAL SOCIETY

MNRAS **502,** 3012–3020 (2021) doi:10.1093/mnras/stab176
Advance Access publication 2021 January 22

Modelled 3D distribution of OH/IR stars in the Galactic disc

Y. Uno [1]★ H. Imai,[2,3] K. Shinano,[4] H.-H. Qiao,[5,6] J. R. Dawson,[7] S. L. Breen [8] and J. F. Gómez [9]

[1]*Department of Physics and Astronomy, Graduate School of Science and Engineering, Kagoshima University, 1-21-35 Korimoto, Kagoshima 890-0065, Japan*
[2]*Amanogawa Galaxy Astronomy Research Center, Graduate School of Science and Engineering, Kagoshima University, 1-21-35 Korimoto, Kagoshima 890-0065, Japan*
[3]*Center for General Education, Institute for Comprehensive Education, Kagoshima University, 1-21-30 Korimoto, Kagoshima 890-0065, Japan*
[4]*Department of Physics and Astronomy, Faculty of Science, Kagoshima University, 1-21-35 Korimoto, Kagoshima 890-0065, Japan*
[5]*National Time Service Center, Chinese Academy of Sciences, Xi'An, Shaanxi 710600, China*
[6]*Shanghai Astronomical Observatory, Chinese Academy of Sciences, 80 Nandan Road, Shanghai 200030, China*
[7]*Department of Physics and Astronomy and MQ Research Centre in Astronomy, Astrophysics and Astrophotonics, Macquarie University, NSW 2109, Australia*
[8]*SKA Organisation, Jordrell Bank, Macclesfield SK11 9FT, UK*
[9]*Institudo de Astrofisíca de Andalucía (CSIC), Glorieta de la Astronomía s/n, E-18008 Granada, Spain*

Accepted 2021 January 15. Received 2021 January 15; in original form 2020 August 14

ABSTRACT

We have modelled the 3D distribution of OH/IR stars in the Galactic plane, traced by 1612 MHz OH maser sources with classic double horned spectral profiles. We statistically analysed over 700 maser sources detected by the HI/OH/Recombination line survey of the Milky Way (THOR) and the Australia Telescope Compact Array interferometric follow-up observations of the Southern Parkes Large-Area Survey in Hydroxyl (SPLASH). With a simple model constructed from a classical density distribution of stars and luminosity functions of OH maser sources in the Galaxy, we estimate the scale height, or the half thickness of the OH/IR star distribution along the Galactic disc to be 90–290 pc. The simple model also implies that there are ∼4000 OH/IR stars hosting 1612 MHz OH masers along the Galactic Plane. Therefore, next generation telescopes such as the Australian Square Kilometre Array Pathfinder (ASKAP) and SKA Phase 1 will detect about 80 per cent of such OH/IR stars in the Galaxy at a 10 mJy detection limit. Comparing the data of previously detected circumstellar 1612 MHz OH maser sources with those of THOR and SPLASH, the maser source lifetime is estimated to be ∼300 yr. This is likely a lower limit, since non-detections of masers in some cases could be affected by the flux variation of the maser source.

Key words: masers – stars: AGB and post-AGB – stars: winds, outflows – H II regions – Galaxy: disc.

1 INTRODUCTION

The structure of our Galaxy has been recently studied through annual parallax and proper motion measurements of OH, H_2O, CH_3OH, and SiO maser lines, whose hosting sources are associated mainly with newly forming massive stars and long-period variable stars (see reviews of Reid & Honma 2014; Green et al. 2015; Paragi et al. 2015). Thousands of maser sources have been catalogued in a variety of surveys of the Galaxy. In particular, H_2O and CH_3OH masers are bright and can be relatively stable, making them the preferred targets for VLBI astrometry. While a large sample of SiO masers have been detected towards the Galactic plane and bulge (e.g. Izumiura et al. 1999; Deguchi et al. 2000a,b; Messineo et al. 2002; Deguchi et al. 2004a,b; Fujii et al. 2006; Trapp et al. 2018), astrometric VLBI investigations are more difficult due to their weaker and less stable emission, in addition to significant atmospheric fluctuations of interferometric fringes at their emitting radio frequency.

Meanwhile, recent successful VLBI astrometry of OH maser sources (van Langevelde et al. 2000; Vlemmings et al. 2003; Vlemmings & van Langevelde 2007; Orosz et al. 2017) encourages the use of OH masers to reveal the Galactic dynamics, as well as the early and final phases of stellar evolution (see also Imai et al. 2016). There have been ∼ 5000 OH maser sources identified throughout the Galaxy (see the catalogue by Engels & Bunzel 2015, see also reviews by Gray 2012; Etoka et al. 2015). OH maser surveys have been conducted in both targeted and unbiased manners. Those targeted surveys have focused on bright infrared sources in star-forming regions (SFR; e.g. Caswell et al. 2010, 2011; Green et al. 2010, 2011) and evolved stars such as asymptotic giant branch (AGB) and post-AGB stars (e.g. Lindqvist et al. 1992a; Blommaert, van Langevelde & Michiels 1994; Blommaert et al. 1998; Sjouwerman et al. 1998), while unbiased surveys have obtained a genuine OH maser distribution in some portions of the Galaxy (e.g. Sevenster et al. 1997a,b; Caswell 1998; Sevenster et al. 2001; Walsh et al. 2016). The HI/OH/Recombination line survey of the Milky Way (THOR) and the Southern Parkes Large-Area Survey in Hydroxyl (SPLASH) are the largest unbiased surveys for all four ground-state OH lines ever conducted in the Northern and Southern sky, respectively (Dawson et al. 2014; Beuther et al. 2016, 2019). In particular, the latter survey is considered as a pathfinder to the Galactic ASKAP Spectral Line Survey (GASKAP; Dickey et al. 2013), which will soon provide a large (>10 000) OH maser sample within both the Galaxy and in nearby external galaxies (Etoka et al. 2015).

★ E-mail: YuriUNO@icloud.com

1612 MHz (satellite line) OH masers are a unique tracer of intermediate-mass oxygen-rich evolved stars with long-period stellar pulsation. Towards those stars, 1612 MHz OH masers are much brighter than 1665 and 1667 MHz (main line) masers, while these masers show the opposite trend in SFRs (Reid et al. 1981). The circumstellar 1612 MHz OH masers are excited in the outer parts of circumstellar envelopes (CSEs), where H_2O molecules are photodissociated by interstellar ultraviolet radiation to form OH molecules. The physical condition required for maser excitation is different from that in SFRs, in which newly born massive stars are embedded in thick molecular gas clouds. The circumstellar 1612 MHz OH masers often show a double-peaked spectral profile, indicating radial maser beaming in an outer shell of a radially expanding CSEs (see a review by Richards 2012) containing an OH/IR star. Mapping such masers enables us to determine an apparent diameter of the OH maser shell, while monitoring observations can measure a phase-lag of a periodic variation of the red-shifted spectral peak with respect to that of the blue-shifted peak, yielding a true physical diameter of the shell. Combining such high angular resolution and monitoring observations thus makes it possible to geometrically determine distances to the OH/IR stars (Herman & Habing 1985; van Langevelde, van der Heiden & van Schooneveld 1990; van Langevelde et al. 1993; Engels et al. 2015).

An expansion velocity for the outer CSE shell can be derived from the double peaks of a 1612 MHz OH maser spectrum. The expansion velocity is a unique parameter of the CSE, enabling us to estimate the efficiency of radial acceleration of the CSE that may be correlated with the luminosity and the mass-loss rate of the central star, as well as the physical properties of the CSE, such as metallicity. In fact, mean expansion velocities of OH/IR stars differ depending on their locations in the Galaxy (Sjouwerman et al. 1999), possibly tracing the history of star formation activity. A correlation between the expansion velocity and the metallicity has also been confirmed (Goldman et al. 2017).

The distribution of evolved stars in the Galaxy has also been utilized to reveal details of the Galactic dynamics, and stellar evolution. In particular, the scale height for evolved stars such as AGB stars is estimated to be around 200–400 pc in the literature (e.g. Rowan-Robinson & Chester 1987; Habing et al. 1988; Jura & Kleinmann 1992; Jackson, Ivezić & Knapp 2002). While these previous studies used the data of targeted observations, we are able to utilize the unbiased THOR/SPLASH surveys to meaningfully investigate the total distribution of OH/IR stars.

In this paper, we present a statistical analysis of the 1612 MHz OH maser sources identified in the THOR and SPLASH surveys. Section 2 outlines our identification method for OH/IR stars exhibiting double OH spectral peaks, as well as brief summaries of THOR and SPLASH observations and the identified maser sources. Section 3 describes how we derived the scale height of the OH/IR stars using a simple model of the OH maser host sources. Section 4 deals statistically with the physical properties of OH maser sources, such as the CSE expansion velocities. Section 5 discusses these results and the lifetime of both 1612 MHz OH maser sources and their progenitor stars.

2 DATA

2.1 THOR

The THOR survey was conducted with the Very Large Array (VLA) between 2012 and 2015. THOR covered 132 $\deg^2$ of the Galactic Plane: $67.25^\circ > l > 14.35^\circ$, $|b| < 1.25$. The survey observations had an angular resolution (FWHM) between 12.5 and 19 arcsec, and a velocity channel spacing of 1.5 $\mathrm{km\,s^{-1}}$. The rms noise level per channel was typically $\sim$10 $\mathrm{mJy\,beam^{-1}}$. The detection limit was 2σ, and the resulting catalogue was presented by Beuther et al. (2016, 2019). A total of 1080 maser spots associated with 621 distinct maser sites were confirmed at 1612 MHz by these authors. Among the distinct maser sites, 68 per cent (422/621) sources were classified as OH/IR stars for use in this work.

Table 1. The coverage and number of 1612 MHz detections of THOR (Beuther et al. 2016, 2019) and SPLASH (Qiao et al. 2016b, 2018, 2020) catalogues.

	THOR	SPLASH
l	$67.25^\circ > l > 14.35^\circ$	$10^\circ > l > -28^\circ$
b	$\|b\| < 1.25^\circ$	$\|b\| < 2^\circ$, $2^\circ < b < 6^\circ$ ($4^\circ > l > -2^\circ$)
Covered area	132 $\deg^2$	176 $\deg^2$
Maser spots	1080	1668
Maser sites	621	752

2.2 SPLASH

The original SPLASH survey was conducted with the Parkes 64 m telescope during 2012–2014. SPLASH covered 176 $\deg^2$ of the Galactic Plane: $10^\circ > l > 4^\circ$, $|b| < 2^\circ$; $4^\circ > l > -2^\circ$, $-2^\circ < b < 6^\circ$; $-2^\circ > l > -28^\circ$, $|b| < 2^\circ$. The survey observations had an angular resolution of 12.2–12.6 arcmin (with an effective resolution of $\sim$ 15 arcmin in the final gridded cubes), and a velocity channel spacing of 0.18 $\mathrm{km\,s^{-1}}$. The rms noise level was typically $\sim$ 65 mJy in the point-source-optimized cubes generated for the purposes of maser searching and the detection limit was 3σ. Later (2013–2016), follow-up observations were conducted with the ATCA to localize these identified masers more accurately. The synthesized beam size ranged from 6.5×4.4 to 20×7 $\mathrm{arcsec^2}$, and the velocity channel spacing was 0.09 $\mathrm{km\,s^{-1}}$. The covered velocity range was about -300 $\mathrm{km\,s^{-1}}$ to $+300$ $\mathrm{km\,s^{-1}}$ in the local-standard-of-rest (LSR) velocity frame. The rms noise level was typically $\sim$70 mJy in each 0.09 $\mathrm{km\,s^{-1}}$ channel. Following the classification of the detected emission made by Qiao et al. (2016b, 2018, 2020), 1668 maser spots associated with 752 distinct maser sites were confirmed in the ATCA follow-up data at 1612 MHz. Note that 27 candidates were detected only with Parkes and they are not included in our data statistics. Among the distinct maser sites, 76 per cent (573/752) sources were classified as OH/IR stars for use in this work.

2.3 Our sample

Our sample of OH/IR stars has been taken from the THOR (Beuther et al. 2016, 2019) and SPLASH (Qiao et al. 2016b, 2018, 2020) catalogues. Both the THOR and SPLASH surveys targeted the four ground-state lines of OH at 1612.231, 1665.402, 1667.359, and 1720.530 MHz. The coverage and number of 1612 MHz detections in these observations are summarized in Table 1.

We define our sample of OH/IR stars by the presence of 1612 MHz OH maser source associated either with a known evolved star from the literature, or with a red, star-like object in GLIMPSE mid infrared images. Note that in contrast to the original catalogue classifications, we do not include any source with only one spectral peak in our definition. For our statistical analysis, we define a 'statistics field' ($67.25^\circ > l > 14.35^\circ$ and $10^\circ > l > -28^\circ$, $|b| < 1.25^\circ$), i.e. restricting the Galactic latitude to the narrower range included in

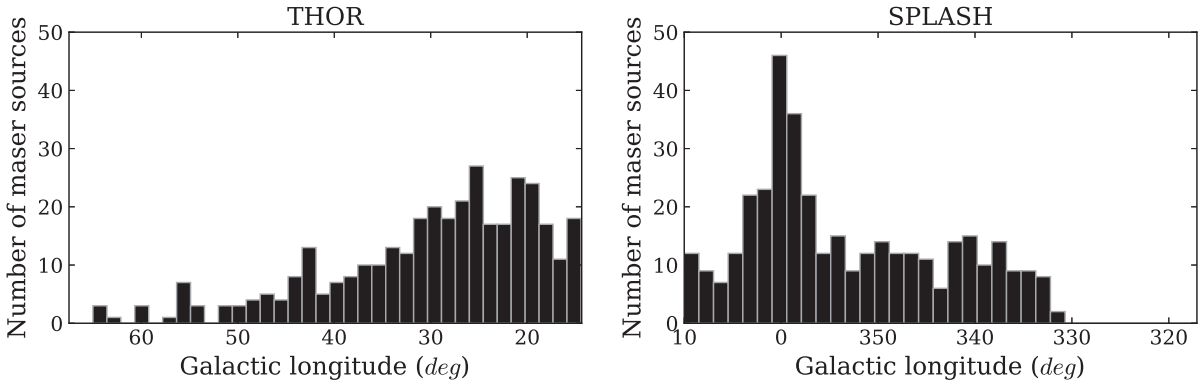

Figure 1. Histogram of the 729 maser sources classified as OH/IR stars as a function of Galactic longitude. The left-hand and right-hand panels show the distributions of OH/IR stars in THOR ($67.25^\circ > l > 14.35^\circ$, $|b| < 1.25^\circ$) and SPLASH ($10^\circ > l > -28^\circ$, $|b| < 1.25^\circ$), respectively. For a proper comparison between both surveys, the maser sources with a flux density lower than the modified SPLASH detection limit (122 mJy) are removed from THOR data.

THOR so that the latitude coverage for THOR and SPLASH sources are homogeneous. We also note that the THOR survey is more sensitive than SPLASH. Therefore, a simple combination of sources would introduce a bias, with comparatively more detected sources in the north. Moreover, the spectral resolution of THOR is coarser than that of SPLASH, resulting in systematic lower flux densities of masers. To mitigate any bias due to these different sensitivities and spectral resolutions of both surveys, we removed from our analysis the THOR sources with peak flux density lower than the modified SPLASH detection limit (δ_s*, 122 mJy) defined as

$$\delta_s* = k\frac{\delta_s}{\upsilon_t}, \tag{1}$$

where k is the typical velocity width of OH maser spectrum (0.94 km s^{-1} , see Section 5.1 for a determination of this value), δ_s is the SPLASH detection limit (65 mJy $\times\, 3\sigma$ = 195 mJy), and υ_t is the velocity resolution of THOR (1.5 km s^{-1}), in order to mitigate any bias due to the different sensitivity and velocity resolution of both surveys. Following these criteria, we select a total of 729 out of the 1373 catalogued maser sources within the statistics field. Fig. 1 shows a histogram of the OH/IR stars as a function of Galactic longitude. The 1612 MHz OH masers are roughly uniformly distributed in the whole statistics field, except for a crowded region within $\sim 4^\circ$ of the GC. This is likely attributed to the Galactic bulge or intrinsic concentration of the maser sources towards the GC.

3 SCALE HEIGHT OF OH/IR STARS IN THE GALACTIC DISC

Because our source is unbiased (and only limited by flux density), we can attempt to estimate the thickness of the distribution of OH/IR stars in the Galactic disc. One way to estimate the scale height (i.e. the typical half thickness of the distribution) is to measure the distances to these sources individually, and then derive their absolute heights above the mid-plane of the disc from their Galactic coordinates. Usually, a kinematic distance method is used to estimate the distances to the individual sources from their radial velocities with a Galactic rotation curve. For OH maser sources, this approach has some shortcomings. First, there is an ambiguity, since two distances (far and near) are compatible with the same radial velocity for sources inside the solar circle. Also, this method cannot be applied to stars close to $l = 0^\circ$, even though the systemic stellar velocity of a maser source with a clear double-horned spectral profile is well determined. Moreover, the kinematics of the evolved stellar population exhibits large random motions, significantly deviating from Galactic circular rotation to a greater degree than the young population (Lindqvist et al. 1992a). Note that the trigonometric parallax distances to OH/IR stars derived by *Gaia* often have large uncertainties, due to their developed CSEs causing asymmetry of the observed starlight distribution or heavy extinction of the starlight (e.g. Matsuno et al. 2020). All these factors affect the accurate estimation of the scale height.

Here we take an alternative approach, constructing simple models of the Galactic disc, to reproduce the positional and flux distribution of the OH maser sources in the THOR/SPLASH field. We adopt an exponential disc model (Jurić et al. 2008) for the stellar distribution along the Galactic plane, and $\mathrm{sech}^2(\frac{a}{\sqrt{2}}z)$ (where a is a constant) model for the direction perpendicular to the Galactic plane (Spitzer 1942; Bahcall 1984), which is approximated to a Gaussian distribution density function for simplicity (Habing et al. 1988):

$$\frac{\mathrm{d}f(z)}{\mathrm{d}z} = \frac{1}{h\sqrt{\pi}}\exp\left(-\frac{z^2}{h^2}\right), \tag{2}$$

where h is the disc scale height.

The peak flux density of each modelled maser source, $F_{\rm peak}$ (defined as the highest flux density value in a double-horned spectrum) is calculated using the equation,

$$F_{\rm peak} = \frac{L_v}{4\pi D^2} \simeq \frac{L_v \times 10^{26}}{4\pi D^2}\,[\mathrm{Jy}]\,, \tag{3}$$

where L_v [W Hz^{-1}] is the luminosity of the OH maser source, and D [m] the distance to the maser source from the Sun's position set to R_0 = 8.2 kpc from the GC and 17 pc above the disc plane (e.g. Karim & Mamajek 2017; Abuter et al. 2019; Reid et al. 2019). In order to assign a certain luminosity to each modelled maser source, we draw test stars at random from the circumstellar OH maser luminosity function of Engels & Bunzel (2015),

$$f(\log(L_v)) = \frac{1}{\sqrt{2\pi\sigma^2}}\exp\left(-\frac{(\log(L_v) - \overline{\log(L_v)})^2}{2\sigma^2}\right), \tag{4}$$

where $\overline{\log(L_v)}$ = 15.3 or 15.5 for near or far kinematic distance stars, respectively, with a dispersion σ = 0.53 for both kinematic distances. Here, because we find the results do not change greatly, we adopt the luminosity function derived from the near kinematic distance stars.

Simple models were constructed from a variety of disc thicknesses and radii (scale lengths of the exponential disc model), incrementing

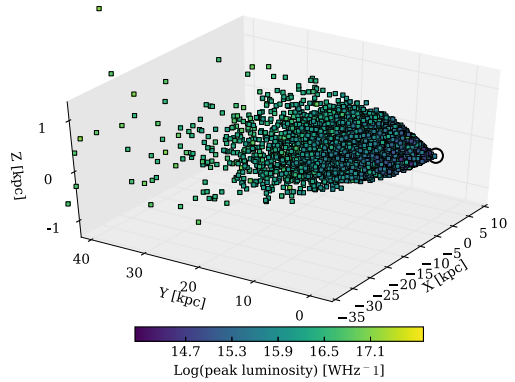

Figure 2. Example of the simulated distribution of the 1612 MHz OH masers (scale height = 150 pc, scale length = 15 kpc). The *Y*-axis is set along the distance from the Sun in the direction of the GC. The *X* and *Z* axes are set along the Galactic longitude and latitude axes, respectively. The circle marks the Sun's position at [*X*, *Y*, *Z*] = [0, 0, 0].

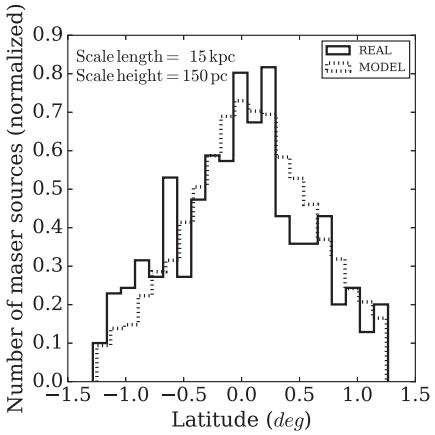

Figure 3. Histograms of the 1612 MHz OH maser distribution in the statistics field, excluding the GC ($|l| < 4°$), as a function of Galactic latitude. The vertical scale indicates the number of maser sources in a specific bin of Galactic latitude. The number of maser sources is normalized so that the total area of the histogram is set to unity. The dotted line shows the simulated distribution profile (*p*-value = 1.0) when the scale length and scale height are 15 kpc and 150 pc, respectively.

in steps of 10 pc and 1 kpc, respectively, using 10^5 test stars (although the real number of OH maser sources in the Galaxy is unknown, see also Section 5). The number of stars were chosen empirically so that its randomness does not affect the results. Each model was then used to generate a synthetic latitude distribution of all detectable sources above the detection limit (122 mJy, see equation 1), which was then compared with the real observed distribution. An example of a simulated 3D maser distribution is presented in Fig. 2 and an example of a histogram profile of the real and simulated OH/IR star distributions is shown in Fig. 3. Note that we excluded all sources within $|l| < 4°$ to remove the distribution of OH/IR stars towards the GC (See Section 2).

The Kolmogorov–Smirnov test (K–S test) was applied to evaluate the compatibility of the observed and modelled distributions. Fig. 4 shows the K–S test results according to different model parameters. We then obtain an OH/IR star scale height of between 90 and 290 pc at a 90 per cent confidence level. Our estimation is slightly lower than the traditional estimated scale heights of evolved stars; 200–400 pc.

For comparison, we also tried to estimate the disc scale height using a kinematic distance method. We adopted the Monte Carlo kinematic distance method of Wenger et al. (2018) with the rotation curve of Reid et al. (2019). The stellar velocity was approximated as the mean peak velocity of the double-horned spectra. The LSR velocity uncertainty was uniformly set to 4.0 km s^{-1} according to the median value of the LSR velocity uncertainty v_u of the full sample of OH/IR stars. For each source, v_u is defined as

$$v_u = \frac{(v_{b_{max}} + v_{r_{max}}) - (v_{b_{min}} + v_{r_{min}})}{2}, \quad (5)$$

where $v_{b_{max}}$ and $v_{r_{max}}$ are the highest velocities of the blue and red peaks, $v_{b_{min}}$ and $v_{r_{min}}$ are the lowest.

Fig. 5 shows the histogram of the distances to the OH/IR stars from the mid-plane of the Galactic disc, derived from the kinematic distances. The two obvious outliers at −612 pc and 1 kpc in the far kinematic distance case are removed. Then we fitted these histograms with Gaussian distributions. From derived values; μ (the location of the peak of the Gaussian distribution) and σ (the standard deviation), scale height is obtained by,

$$h = \sqrt{\mu^2 + 2\sigma^2}. \quad (6)$$

We obtained $\mu = 12 \pm 3$ pc, $\sigma = 37 \pm 2$ pc, and $\mu = 30 \pm 10$ pc, $\sigma = 153 \pm 8$ pc for the two extreme cases where all the sampled stars are at near and far kinematic distances, respectively. Here, stars outside the Solar circle are included in the far kinematic distance group. The derived scale heights assuming the two extreme cases are 54 and 218 pc, respectively.

The distribution of the OH/IR stars in the Galactic plane obtained from kinematic distances is shown in Fig. 6. We plot all sources twice: at both their nearside and farside distances. We could not derive distances for 8.3 per cent (48/575) of the stars within the Solar circle and 5.6 per cent (32/575) of the sources outside the Solar circle because they have too low negative or high positive velocities. As seen in Fig. 6, we find some sources outside the Solar circle beyond the Galactic centre.

4 CSE EXPANSION VELOCITIES OF DOUBLE-HORNED MASER SOURCES

Many studies have attempted to study the astrophysical implications of the derived parameters of the double-horned spectral profiles of 1612 MHz OH masers associated with CSEs around OH/IR stars. Fig. 7 shows a histogram of CSE expansion velocities derived from the half velocity separations between the spectral double peaks of the maser sources in the statistics field. Their mean and median values are both 15 km s^{-1} . The histogram profiles shown in both Figs 1 and 7 are similar to those derived from the Galactic OH masers catalogued by Engels & Bunzel (2015) which were constructed using combination of data obtained from both targeted and unbiased surveys.

Conventionally, OH maser distributions are compared by dividing a sample into low and high expansion velocity groups whose group boundary is set to the mean value (15 km s^{-1}). For instance, Lindqvist, Habing & Winnberg (1992b) found the high expansion velocity group is located closer to the Galactic plane than the low expansion velocity group. Taking into account the correlation between the stellar luminosity and the CSE expansion velocity (Nguyen-Q-Rieu, Winnberg & Schultz 1979; Goldman et al. 2017), the progenitors of OH/IR stars with low expansion velocity are expected statistically to have lower stellar masses and longer lifetimes. This supports the different Galactic distributions of the two groups.

Fig. 8 shows the distribution of OH/IR stars in the statistics field as

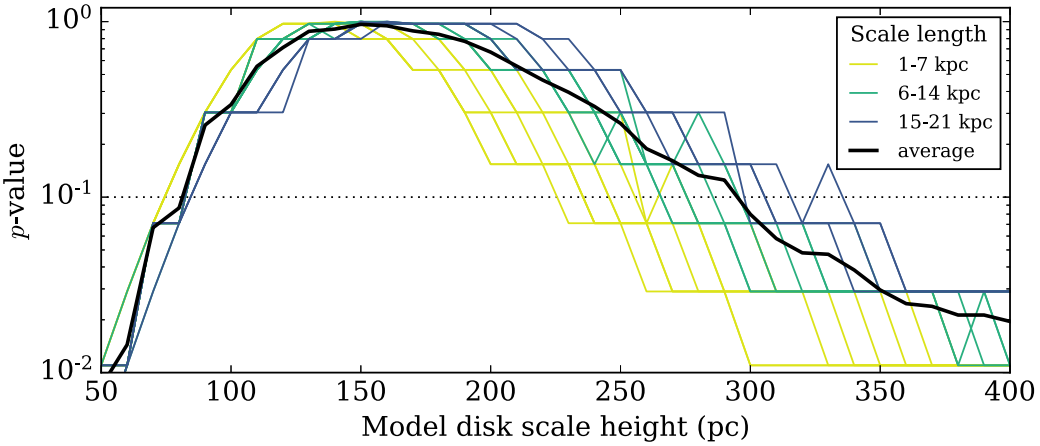

Figure 4. *p*-values resulting from the K–S tests according to scale height and Galactic disc radius. The vertical axis is truncated at 10^{-2}. The dotted line shows the 90 per cent of confidence level. The thick line represents the average *p*-value of models with different scale lengths respect to scale heights. Scale heights of 90 to 290 pc are consistent with our data for a 90 per cent confidence level.

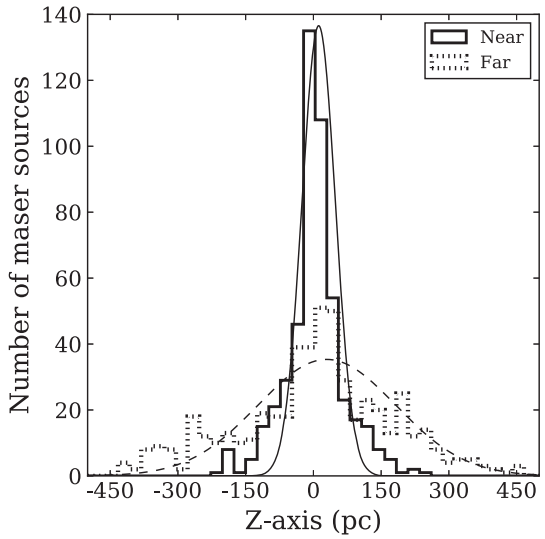

Figure 5. Distribution of OH/IR stars in the statistics field, excluding the GC ($|l| < 4°$) as a function of vertical distance from the Galactic mid-plane, assuming near or far kinematic distances, and obtained from the Monte Carlo kinematic distance method of Wenger et al. (2018). The disc scale heights derived from the fitted Gaussian distributions are 54 pc for near and 218 pc for far kinematic distances.

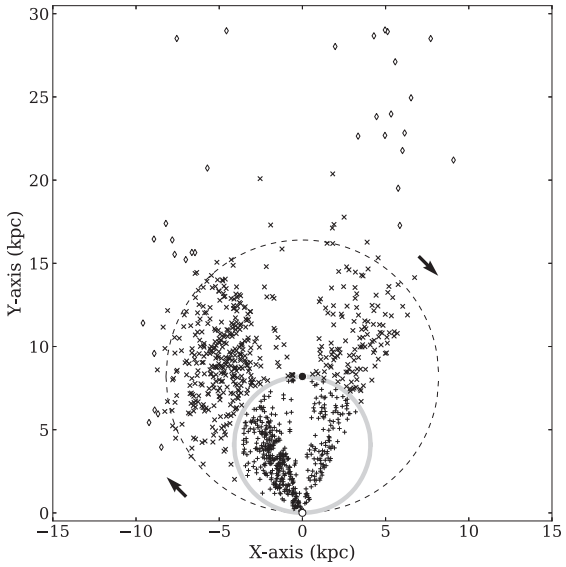

Figure 6. 2D distribution of OH/IR stars in the statistics field on the Galactic plane, excluding the GC ($|l| < 4°$). The white circle marks the Sun's position at X, Y = [0, 0], and the black circle the centre of the Galaxy at [0, 8.2]. The solid circle connects the Sun and the Galactic Centre. The dotted circle shows the solar circle. All sources within the solar circle are plotted at both their near and farside distances: ' + ' and 'x' symbols denote the near and far kinematic distance solutions, respectively. Diamonds denote stars located outside the solar circle.

a function of Galactic latitude in the two different expansion velocity groups. The distribution of the high expansion velocity group looks symmetric with respect to the Galactic mid-plane, which is expected for a uniform distribution in the Galactic plane. Here remember that the Sun sits at +17 pc above the mid-plane. If the maser sources are located in the Galactic plane, we expect that their distribution to be biased towards negative Galactic latitudes. The distribution of the high expansion velocity group looks marginally consistent with this bias. On the other hand, one can see a positive bias in the Galactic latitude for the low expansion velocity group. This bias may indicate the presence of a larger population of OH/IR stars with lower masses and luminosities associated with the warped Galactic disc (Nakanishi & Sofue 2016), but this should be further investigated.

5 DISCUSSION

5.1 Lifetime of circumstellar OH maser sources

Engels & Jiménez-Esteban (2007) suggest that the duration of the OH/IR star phase emitting OH masers can be estimated by analysing the permanent deaths of OH maser sources due to their evolution. They derive the following equation to estimate the probability that *m* out of a sample of *n* stars hosting maser emission will lose their emission in a time interval of ΔT if the lifetime of maser activity in

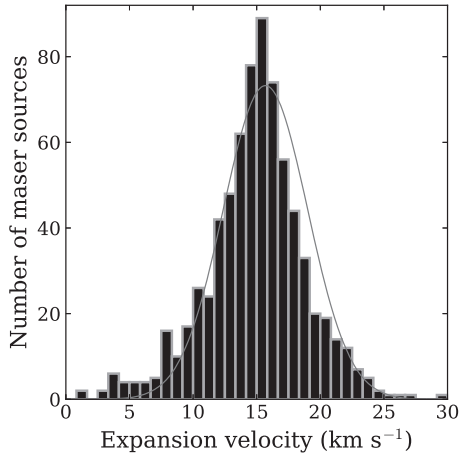

Figure 7. Histograms of expansion velocities of the double-peaked spectra of the OH maser sources ($N = 729$) in the statistics field. Gaussian distributions fitted to the histogram is shown in a solid line ($\mu_e = 15.6 \pm 0.1$ km s^{-1}, $\sigma_e = 3.2 \pm 0.1$ km s^{-1}).

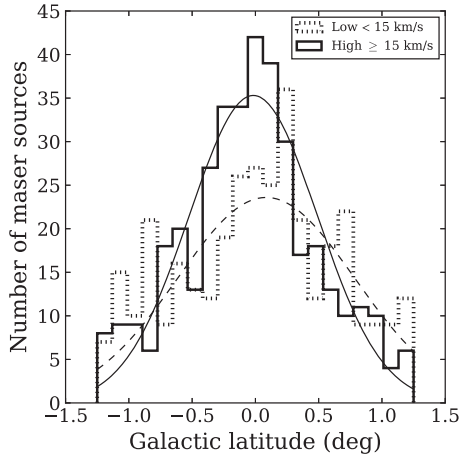

Figure 8. Histograms of OH maser source distributions according to two different expansion velocity groups as a function of Galactic latitude. The maser sources are grouped into the one with low expansion velocities (<15 km s^{-1}, a thick dotted line, $N = 350$) and high expansion velocities (≥ 15 km s^{-1}, a thick line, $N = 379$). Gaussian distributions fitted to these histograms are shown in a dotted line ($\mu_l = 0.13 \pm 0.08\,^\circ$, $\sigma_l = 0.70 \pm 0.07\,^\circ$) and a solid line ($\mu_l = 0.02 \pm 0.04\,^\circ$, $\sigma_l = 0.51 \pm 0.03\,^\circ$).

each CSE is T:

$$P_m^n = \frac{n!}{m!(n-m)!}\left(\frac{\Delta T}{T}\right)^m\left(1-\frac{\Delta T}{T}\right)^{n-m}. \quad (7)$$

In order to determine this lifetime, we checked the number of OH/IR stars within the THOR/SPLASH survey area whose OH emission has disappeared in the ∼20 yr that have elapsed since the survey of Sevenster et al. (1997a,b, 2001). To this end, we cross-matched the double-peaked sources in Sevenster et al. (1997a,b, 2001) with 1612 MHz maser sources detected in THOR/SPLASH across the common covered areas ($45^\circ > l > 14.3^\circ$, $|b| < 1.25^\circ$; $10^\circ > l > 4$, $|b| < 2^\circ$; $4^\circ > l > -2^\circ$, $-2^\circ < b < 3^\circ$; $-2^\circ < l < -28^\circ$, $|b| < 2^\circ$). We consider a source match when there is a detection both in Sevenster et al. and THOR/SPLASH, with a reported position in the former within the beam of the latter (18 arcsec for VLA and ATCA, 12 arcmin for Parkes).

Table 2. List of double-peaked OH sources at 1612 MHz in Sevenster et al. (1997a,b, 2001) that did not show a double-peaked profile in THOR/SPLASH data or were found not to be OH/IR stars. A – single-peaked; SF – star formation region; St – star; P – planetary nebula; O – detected only with Parkes; U – unknown.

OH039.916+00.018 (A)	OH016.398−00.774 (U)
OH037.187+00.090 (A)	OH014.622+00.684 (SF)
OH032.130+00.935 (A)	OH008.483+00.176 (A)
OH031.649−01.082 (A)	OH005.885−00.392 (SF)
OH030.944+00.035 (SF)	OH004.565−00.130 (A)
OH030.270+00.632 (U)	OH000.892+01.342 (P)
OH029.446−00.677 (SF)	OH000.667−00.035 (SF)
OH028.128−00.638 (A)	OH000.517+00.050 (A)
OH026.434−01.077 (A)	OH000.207+01.414 (A)
OH025.057−00.350 (A)	OH359.978+02.563 (A)
OH024.993−00.150 (A)	OH359.857+01.005 (A)
OH024.581+00.224 (U)	OH359.429+00.036 (A)
OH023.937−00.152 (A)	OH356.662+00.113 (O)
OH023.480−00.866 (U)	OH354.642+00.830 (A)
OH022.445+00.036 (A)	OH354.104−01.982 (A)
OH021.996+00.072 (A)	OH353.945−00.972 (O)
OH020.679+00.084 (A)	OH353.747−01.541 (O)
OH019.554−00.172 (A)	OH353.637+00.815 (O)
OH017.551−00.126 (St)	OH351.774−00.536 (SF)
OH017.008−01.226 (A)	–

In total, 427 out of 464 double-peaked sources reported by Sevenster et al. (1997a,b, 2001) had a counterpart in the THOR/SPLASH data. Most of them (388/427) were also double-peaked in THOR/SPLASH. The remaining 39 sources which did not show a double-peaked profile are listed in Table 2. In 23 out of the 39 matches, the spectra appeared as single-peaked in THOR/SPLASH, but we still consider them as OH/IR candidates. We also found that some sources (5/39) were detected with the Parkes telescope, but not with ATCA (see Table 2). On the other hand, we found a few sources that were actually associated with SFRs (6/39), star of unknown type (1/39), or planetary nebula (1/39) and unknowns (4/39). These 12 sources were then excluded from the lifetime estimation.

Regarding the 37 sources for which we did not find any counterpart (Table 3), we investigated whether their non-detection in THOR/SPLASH was due to insufficient sensitivity and/or maser variability. With a typical rms noise in THOR/SPLASH data, in principle all sources except OH346.505−00.052 should be above the detection limit. Fig. 9 shows the comparison of the observed flux densities of our sources with their flux densities as reported by Sevenster et al. (1997a,b, 2001). As already noted by Beuther et al. (2019) and Dawson et al. (2014), the flux densities in THOR/SPLASH appear systematically brighter (by a factor of ∼1.32 for THOR, and ∼1.56 for SPLASH) than those in Sevenster et al., as expected from the coarser spectral resolutions of the latter surveys (2.27 km s^{-1} for Sevenster et al. (2001) – covering the THOR survey region – and 1.46 km s^{-1} for Sevenster et al. (1997a,b) – for the SPLASH survey region). In particular, the systematically higher flux densities measured as a result of the very narrow spectral resolution of SPLASH allow calculation of the typical velocity width of a maser spectrum k given by,

$$k = \frac{1.46}{1.56} = 0.94 \text{ kms}^{-1}. \quad (8)$$

Once the differing spectral resolutions are properly accounted for, THOR/SPLASH should have sufficient sensitivity to detect all sources in Table 3. Another possible explanation for the non-detections is intrinsic maser variability. The maser emission in OH/IR

Table 3. List of sources detected in Sevenster et al. (1997a,b, 2001), but not in THOR/SPLASH. F_p is the reported maximum flux density (either the blue or red peak). The comment column shows the sources whose non-detections in SPLASH can be explained by periodic variability (V) or possible permanent disappearance (U).

Name	F_p (Jy)	v_{exp} (km s^{-1})	Comment
sOH039.093+00.941	0.49	11.4	U
OH032.731−00.327	4.25	14.8	U
OH031.219+01.133	0.44	13.6	U
OH031.091−00.686	1.58	19.3	U
OH030.336+01.171	0.24	5.7	U
OH027.576−00.347	0.45	13.6	U
OH027.047+01.116	0.30	15.9	U
OH025.544−00.606	0.19	9.1	U
OH017.206−01.098	0.69	12.4	U
OH014.634−00.688	0.29	13.6	U
OH014.431−00.033	0.63	2.2	U
OH009.877−00.128	0.42	16.1	U
OH008.885−00.516	0.77	16.8	U
OH006.736−00.473	0.65	8.0	U
OH005.481+01.066	0.22	7.3	V
OH003.253−01.468	0.24	17.5	V
OH002.140−00.373	0.52	17.5	U
OH001.155−00.029	0.43	11.0	U
OH001.134−00.062	0.47	13.1	U
OH000.729+00.451	0.64	5.1	U
OH000.523−00.667	0.82	78.8	U
OH359.117−00.169	0.53	21.2	U
OH358.255+03.184	0.80	8.8	U
OH355.641−01.742	4.03	10.2	U
OH355.091−00.954	0.62	13.1	U
OH354.968−01.066	0.77	8.8	U
OH352.135−01.369	0.29	15.3	V
OH351.607+00.022	0.33	18.3	V
OH349.905−00.451	0.45	15.3	U
OH349.532−00.378	0.43	4.4	U
OH346.505−00.052	0.18	16.8	V
OH341.259+00.458	0.30	16.8	V
OH340.042−00.092	0.25	17.5	V
OH338.456−00.188	0.70	27.7	U
OH338.387+00.725	0.79	13.1	U
OH338.223+00.461	1.64	13.1	U
OH336.451−00.053	0.79	16.1	U

stars is usually periodically variable, with amplitude variation by a factor of three (e.g. Harvey et al. 1974; Engels et al. 2015, 2018). Fig. 10 shows the distribution of the ratio between the flux densities measured by THOR/SPLASH and Sevenster et al. (1997a,b, 2001). Almost all the sources (398/411) have values of logarithm of ratios between −0.5 and 0.5, corresponding to ratios between a factor of 3. This indicates that the amplitude of variability of OH maser emission in OH/IR stars is typically lower than a factor 3.

Taking into account the trend for weaker peak flux density and the possible flux variability in Sevenster et al. (1997a,b, 2001) and the flux variability (here, we adopt a factor of three for periodic variability), the maser sources that were potentially not detectable in THOR/SPLASH due to sensitivity limitations and/or variability are those with a flux density F_v below the limit

$$F_v < \frac{\delta}{w} \times \text{variability}, \tag{9}$$

where δ is detection limit (2σ; 20 mJy for THOR and 3σ; 195 mJy for SPLASH) and w is weighting factor (1.32 for THOR and 1.56 for SPLASH). We have found the seven sources apply such case, marked

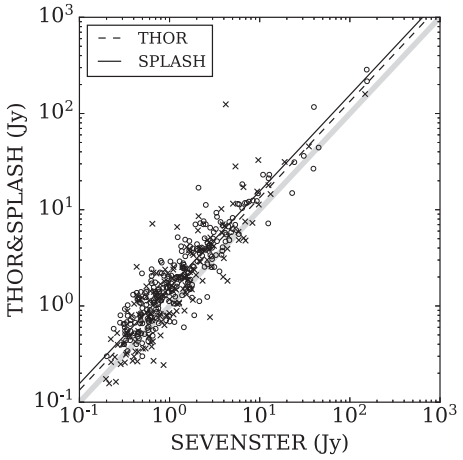

Figure 9. Relationship of peak flux density of OH maser sources in Sevenster et al. (1997a,b, 2001) and THOR/SPLASH. The thick grey line represents where the points would lie if all sources showed the same flux densities in both surveys. The dotted line represents the best linear fit between the flux densities in THOR and Sevenster et al. (2001). The solid line represents an equivalent fit for the SPLASH and Sevenster et al. (1997a,b) data. Individual sources from THOR and SPLASH data are represented as 'x' and 'o', respectively.

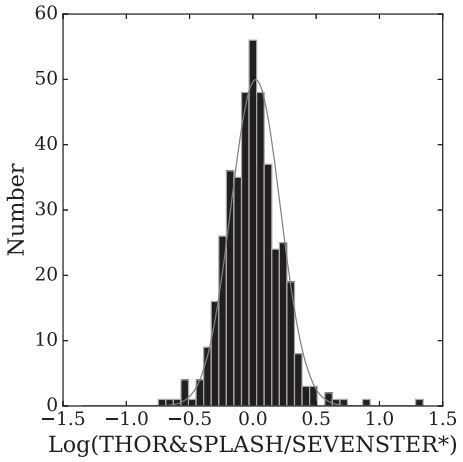

Figure 10. Histogram of peak flux density ratio, THOR/SPLASH to Sevenster et al. (1997a,b, 2001). Here, the later peak flux density is multiplied by 1.56 for Sevenster et al. (1997a,b), and 1.32 for Sevenster et al. (2001) (see SubSection 5.1). The x-axis is the natural logarithm of the flux density ratio. The grey line represents a Gaussian distribution fitted to the histogram ($\mu_r = 0.022 \pm 0.005$, $\sigma_r = 0.196 \pm 0.004$).

with 'V' in Table 3. This indicates 1.5 per cent (7/452; 464 minus 6 SFRs, 1 star, 1 planetary nebula, and 4 unknowns) of maser sources may have not been detected by THOR/SPLASH because of their intrinsic variability. Note that 57.2 per cent (519/907) of the OH/IR stars detected in THOR/SPLASH were not detected in Sevenster et al. (1997a,b, 2001).

In summary, the total number of target sources used in our OH maser lifetime estimation was 445 (464 minus the 7 potentially variable sources, 6 SFRs, 1 star, 1 planetary nebula, and 4 unknowns). Therefore, as inputs for equation (7) we have $n = 445$, $m = 30$ (the 37 in Table 3 minus 7 marked with 'V'), $\Delta T \sim 20$ yr (1993–2015). From these values, we then estimate a lifetime of $T \sim 300$ yr for OH emission in OH/IR stars. This is very similar to the lifetime (313 yr) derived by Lewis (2002) but much shorter than the duration

Table 4. Number of detectable OH/IR stars in the Galactic disc estimated from our model on conditions of THOR/SPLASH and SKA observations assuming their detection limit 230 and 10 mJy each. 'All' means the total number of OH/IR stars in the modelled Galactic disc. 'Detectable' and 'Statistics' represent the numbers of detectable OH/IR stars in the Galactic disc and the statistics field (see Section 2 for its definition), respectively.

Facility	All	Detectable	Statistics
THOR/SPLASH	3990	1434 (36 per cent)	728 (18 per cent)
SKA Phase 1	3990	3210 (80 per cent)	1543 (39 per cent)

of the super wind phase (1000–4000 yr; Lewis 2001) and the lower limit to the OH maser lifetime associated to OH/IR stars (>3000 yr) calculated by Engels & Jiménez-Esteban (2007). They noted that the sampling of different types of OH/IR stars can result in different derived lifetimes. In fact, most of the disappeared maser sources of Lewis (2002) are low-mass AGB stars ($v_{\rm exp} < 12\,{\rm km\,s^{-1}}$) while Engels & Jiménez-Esteban (2007) targeted more massive AGB stars ($v_{\rm exp} > 12\,{\rm km\,s^{-1}}$) which may have more stable OH maser environment supported by denser envelopes (Engels & Jiménez-Esteban 2007). In contrast, as seen in Table 3, our disappearing maser sources cannot be constrained to low-mass main sequence stars on the basis of their expansion velocities. Therefore another explanation might be needed for the discrepancy. Nevertheless, our estimate is somewhat uncertain since, for instance, some of the undetected sources may have a variability with a larger amplitude than assumed, and may reappear at a later time, which would make the estimated time longer. In any case, the cause of our non-detections will have to be investigated more carefully.

5.2 Comparison of the scale heights of star distributions among different stellar types

In this paper, we estimated the thickness of the Galactic distribution of OH/IR stars, obtaining a scale height of 100–200 pc. In literature, the scale height of O–B type stars is reported to be between 30 and 100 pc (Jesús 2001; Da-Li & Zi 2008). The scale heights of A–F type and G–K type stars are reported to be around 100–200 pc (de Souza & Teixeira 2007) and 300–700 pc (Siebert, Bienaymé & Soubiran 2003; Guo 2020), respectively. These imply that the majority of OH/IR stars have lifetimes equivalent to those of A–F type stars. In order to discuss whether OH/IR stars have lifetimes as long as those of lower mas G–M type stars, it is necessary to conduct deeper surveys of circumstellar OH masers associated with such stars.

5.3 Census of OH/IR stars in the Galactic plane

Our simple model can roughly reproduce the distribution of OH/IR stars in the Galactic disc from two parameters: a scale height and a radial scale length. We choose a scale height of 150 pc for which one of the highest score was obtained in the K–S test (see Section 3), and assume a radial scale length of 22 kpc (the galactocentric distance of the farthest SFR confirmed to date; Brand & Wouterloot 2007; Izumi et al. 2014) with the luminosity function obtained using the near kinematic distances. By equalizing the number of OH/IR stars in the Galactic disc model in the area covered by THOR/SPLASH with that of the actual OH/IR stars detected by THOR/SPLASH. We obtain the population of OH/IR stars in the Galaxy. We estimate a total of ∼4000 OH/IR stars for a scale height of 150 pc. Table 4 summarizes the estimated number of detectable sources with the sensitivity of THOR/SPLASH and ASKAP/SKA Phase 1 (assuming the whole sky were accessible to them). Thus, next-generation telescopes will be able to reach 80 per cent completeness at a detection limiting 10 mJy, effectively producing a census of OH/IR stars in order to estimate the lifetime of stars becoming OH/IR stars more precisely. This estimation is consistent with that by Etoka et al. (2015).

ACKNOWLEDGEMENTS

We thank an anonymous referee, Dieter Engels and Ross A. Burns for kind advices making our work better. For deriving a kinematic distance, we used a python library provided by Trey Wenger (https://github.com/tvwenger/kd). This research has made use of: NASA's Astrophysics Data System Abstract Service; NASA/IPAC Infrared Science Archive, which is funded by the National Aeronautics and Space Administration and operated by the California Institute of Technology; and Database of Circumstellar Masers. HI was supported by the Bilateral Collaboration Program by the Japan Society for Promotion of Science (JSPS) and KAKENHI programs 25610043 and 16H02167 by the Ministry of Education, Culture, Sports, Science and Technology (MEXT). JFG and HI were supported by the Invitation Program for Foreign Researcher by JSPS (S14128), by Amanogawa Galaxy Astronomy Research Center (AGARC), and the State Agency for Research of the Spanish MCIU through the 'Center of Excellence Severo Ochoa' award for the Instituto de Astrofísica de Andalucía (SEV-2017-0709). JFG also acknowledges support by MCIU-AEI (Spain) grant AYA2017-84390-C2-R (co-funded by FEDER). JRD acknowledges the support of an Australian Research Council (ARC) DECRA Fellowship (project number DE170101086). H-HQ is partially supported by the Special Funding for Advanced Users, budgeted and administrated by Center for Astronomical Mega-Science, Chinese Academy of Sciences (CAMS-CAS), CAS 'Light of West China' Program and the National Natural Science Foundation of China (Grant No. 11903038).

DATA AVAILABILITY

The data underlying this article are available in the GitHub, at https://github.com/yuriuno/ohirstar-scaleheight-lifetime.

REFERENCES

Bahcall J. N., 1984, ApJ, 276, 156
Beuther H. et al., 2016, A&A, 595, A32
Beuther H. et al., 2019, A&A, 628, A90
Blommaert J. A. D. L., van Langevelde H. J., Michiels W. F. P., 1994, A&A, 287, 479
Blommaert J. A. D. L., van der Veen W. E. C. J., van Langevelde H. J., Habing H. J., Sjouwerman L. O., 1998, A&A, 329, 991
Brand J., Wouterloot J. G. A., 2007, A&A, 464, 909
Caswell J. L., 1998, MNRAS, 297, 215
Caswell J. L. et al., 2010, MNRAS, 404, 1029
Caswell J. L. et al., 2011, MNRAS, 417, 1964
Da-Li K., Zi Z., 2008, Chin. Astron. Astrophys., 32, 360
Dawson J. R. et al., 2014, MNRAS, 439, 1596
de Souza R. E., Teixeira R., 2007, A&A, 471, 475
Deguchi S. et al., 2004a, PASJ, 56, 261
Deguchi S. et al., 2004b, PASJ, 56, 765
Deguchi S., Fujii T., Izumiura H., Kameya O., Nakada Y., Nakashima J.-i., Ootsubo T., Ukita N., 2000a, ApJS, 128, 571
Deguchi S., Fujii T., Izumiura H., Kameya O., Nakada Y., Nakashima J.-i., 2000b, ApJS, 130, 351
Dickey J. M. et al., 2013, Publ. Astron. Soc. Austr., 30, e003
Engels D., Bunzel F., 2015, A&A, 582, A68

Engels D., Jiménez-Esteban F., 2007, A&A, 475, 941
Engels D., Etoka S., Gérard E., Richards A., 2015 , in Kerschbaum F., Wing R. F., Hron J., eds, ASP Conf. Ser. Vol. 497, Why Galaxies Care about AGB Stars III: A Closer Look in Space and Time. Astron. Soc. Pac., San Francisco, p. 473
Engels D., Etoka S., West M., Gérard E., 2018, Astrophysical Masers: Unlocking the Mysteries of the Universe, Proceedings of the International Astronomical Union, IAU, S336 , 13, 389
Etoka S., Engels D., Imai H., Dawson J., Ellingsen S., Sjouwerman L., van Langevelde H., 2015, in Bourke T. L. , et al., Proceedings of Advancing Astrophysics with the Square Kilometre Array (AASKA14), Vol. 125, Available at: https://pos.sissa.it/cgi-bin/reader/conf.cgi?confid=215
Fujii T., Deguchi S., Ita Y., Izumiura H., Kameya O., Miyazaki A., Nakada Y., 2006, PASJ, 58, 529
Goldman S. R. et al., 2017, MNRAS, 465, 403
Gravity Collaboration 2019, A&A, 625, L10
Gray M., 2012, Maser Sources in Astrophysics. Cambridge Univ. Press, Cambridge
Green J., Van Langevelde H. J., Brunthaler A., Ellingsen S., Imai H., Vlemmings W. H. T., Reid M. J., Richards A. M. S., 2015, in Bourke T. L. , et al., Proceedings of Advancing Astrophysics with the Square Kilometre Array (AASKA14), Vol. 119, Available at: https://pos.sissa.it/cgi-bin/reader/conf.cgi?confid=215
Green J. A. et al., 2010, MNRAS, 409, 913
Green J. A. et al., 2011, ApJ, 733, 27
Guo R. et al., 2020, MNRAS, 495, 4828
Habing H. J., 1988, A&A, 200, 40
Harvey P. M., 1973, ApJS, 27, 331
Herman J., Habing H. J., 1985, A&AS, 59, 523
Imai H., Burns R. A., Yamada Y., Goda N., Yano T., Orosz G., Niinuma K., Bekki K., 2016, in Ichiki K. , et al., eds, SKA Japan Science Book
Izumi N., Kobayashi N., YasuiC., Tokunaga A., Saito M., Hamano S., 2014, ApJ, 795, 66
Izumiura H., Deguchi S., Fujii T., Kameya O., Matsumoto S., Nakada Y., Ootsubo T., Ukita N., 1999, ApJS, 125, 257
Jackson T., Ivezić Ž., Knapp G. R., 2002, MNRAS, 337, 749
Jesús M.-A., 2001, AJ, 121, 2737
Jura M., Kleinmann S. G., 1992, ApJS, 79, 105
Jurić M. et al., 2008, ApJ, 673, 864
Karim M. M., Mamajek E. E., 2017, MNRAS, 465, 472
Lewis B. M., 2001, ApJ, 560, 400
Lewis B. M., 2002, ApJ, 576, 445
Lindqvist M., Winnberg A., Habing H. J., Matthews H. E., 1992, A&AS, 92, 43
Lindqvist M., Habing H. J., Winnberg A., 1992, A&A, 259, 118
Matsuno M. et al., 2020, PASJ, 72, 56
Messineo M., Habing H. J., Sjouwerman L. O., Omont A., Menten K. M., 2002, A&A, 393, 115
Nakanishi H., Sofue Y., 2016, PASJ, 68, 5
Nguyen-Q-Rieu L.-M. C., Winnberg A., Schultz G. V., 1979, A&A, 75, 351
Orosz G. et al., 2017, AJ, 153, 119
Paragi Z. et al., 2015, in Bourke T. L. , et al., Proceedings of Advancing Astrophysics with the Square Kilometre Array (AASKA14), Vol. 143, Available at: https://pos.sissa.it/cgi-bin/reader/conf.cgi?confid=215
Qiao H.-H. et al., 2016, ApJS, 227, 26
Qiao H.-H. et al., 2018, ApJS, 239, 15
Qiao H.-H. et al., 2020, ApJS, 247, 5
Reid M. J et al., 2019, ApJ, 885, 131
Reid M. J., Honma M., 2014, ARA&A, 52, 339
Reid M. J., Moran J. M., 1981, ARA&A, 19, 231
Richards A. M. S., 2012, in Booth R.S., Humphrey E. M. L, Vlemmings W. H. T., eds, Cosmic Masers - from OH to H, Vol. 287, IAU Symposium, p. 199
Rowan-Robinson M., Chester T., 1987, ApJ, 313, 413
Sevenster M. N., Chapman J. M., Habing H. J., Killeen N. E. B., Lindqvist M., 1997a, A&AS, 122, 79
Sevenster M. N., Chapman J. M., Habing H. J., Killeen N. E. B., Lindqvist M., 1997b, A&AS, 124, 509
Sevenster M. N., van Langevelde H. J., Moody R. A., Chapman J. M., Habing H. J., Killeen N. E. B., 2001, A&A, 366, 481
Siebert A., Bienaymé O., Soubiran C., 2003, A&A, 399, 531
Sjouwerman L. O., van Langevelde H. J., Winnberg A., Habing H. J., 1998, A&AS, 128, 35
Sjouwerman L. O., Habing H. J., Lindqvist M., van Langevelde H. J., Winnberg A., 1999, in Falcke H., Cotera A., Duschl W. J., Melia F., Rieke M. J., eds, ASP Conf. Ser. Vol. 186, The Central Parsecs of the Galaxy. Astron. Soc. Pac., San Francisco, p. 379
Spitzer L. J., 1942, ApJ, 95, 329
Trapp A. C., Rich R. M., Morris M. R., Sjouwerman L. O., Pihlström Y. M., Claussen M., Stroh M. C., 2018, ApJ, 861, 75
van Langevelde H. J., van der Heiden R., van Schooneveld C., 1990, A&A, 239, 193
van Langevelde H. J., Janssens A. M., Goss W. M., Habing H. J., Winnberg A., 1993, A&AS, 101, 109
van Langevelde H. J., Vlemmings W., Diamond P. J., Baudry A., Beasley A. J., 2000, A&A, 357, 945
Vlemmings W. H. T., van Langevelde H. J., 2007, A&A, 472, 547
Vlemmings W. H. T., van Langevelde H. J., Diamond P. J., Habing H. J., Schilizzi R. T., 2003, A&A, 407, 213
Walsh A. J. et al., 2016, MNRAS, 455, 3494
Wenger T. V. et al., 2018, ApJ, 856, 52

This paper has been typeset from a TEX/LATEX file prepared by the author.